Available online at www.sciencedirect.com
ScienceDirect
Ceramics International 36 (2010) 1143–1146
CERAMICS INTERNATIONAL
www.elsevier.com/locate/ceramint

Short communication

Influence of magnesia on sintering stress of alumina

Takayasu Ikegami [a,*], Nobuo Iyi [b], Isao Sakaguchi [c]

[a] Strategy Office, National Institute for Materials Science, 1-2-1 Sengen, Tsukuba-shi, Ibaraki 305-0047, Japan
[b] Nanoscale Materials Center, National Institute for Materials Science, 1-1 Namiki, Tsukuba-shi, Ibaraki 305-0044, Japan
[c] Optronic Materials Center, National Institute for Materials Science, 1-1 Namiki, Tsukuba-shi, Ibaraki 305-0044, Japan

Received 26 March 2009; received in revised form 3 September 2009; accepted 6 October 2009
Available online 4 November 2009

Abstract

The sintering stress and the densification of MgO-doped Al_2O_3 were measured with a self-loading apparatus and a thermomechanical analyzer, respectively. The densification started at 950 °C and finished at about 1450 °C. The measured surface tensions were 0.7–0.8 N m^{-1} in the intermediate sintering stage but drastically decreased to 0.2 N m^{-1} in the final stage of sintering.

Keywords: A. Sintering; D. Al_2O_3; D. MgO; Driving force

1. Introduction

Coble [1] was the first who fabricated translucent Al_2O_3 ceramics with the aid of a small amount of MgO, and then a lot of applied studies focused on fabrication of transparent ceramics with various additives, such as fluoride-doped MgO [2], silica-doped YAG [3], sulfate ions-doped Y_2O_3 [4], etc. Fundamental studies [5–7] have, also, been successively made to verify the role of additives in densification of ceramics. In particular, the role of MgO [8–11] in densification of Al_2O_3 has been extensively examined.

Doping of MgO has been always valid for complete elimination of pores from Al_2O_3 ceramics. Reported influences of MgO on densification or grain growth of Al_2O_3, however, were controversial. For example, MgO in some papers [8,9] inhibited grain growth of Al_2O_3, thus enabling the pores to stay attached to the moving grain boundaries. Other papers [10,11] indicated no influence of MgO on grain growth of Al_2O_3. Berry and Harmer [12] well summarized the controversial results at the viewpoint of atomic mobility.

Not a few studies have been devoted to measure the diffusion coefficients of oxygen and aluminum in alumina [13–16]. Although the surface tension [17,18] is the driving force for sintering and densification, there have been few papers on the empirical relationship between surface tension and densification [19–21]. This may be attributed to the difficulty in measurement of the surface tension or the sintering force. No empirical relationship between the surface tension of Al_2O_3 and doping MgO has been reported. A self-loading apparatus was developed to measure the sintering force of a powder compact [22]. Automatically inhibiting the axial shrinkage of the specimen, this loading apparatus measures the apparent sintering force without controlling shrinkage of the powder compact. The surface tensions of MgO-doped Al_2O_3 were evaluated from the measured sintering stresses, being compared with those of the undoped Al_2O_3 reported elsewhere [22].

2. Experimental procedures

A commercially available Al_2O_3 powder (TM-DAR, Taimei Chem. Co. Ltd., Nagano, Japan, with impurities of Si = 11–15 ppm, Fe = 9–10 ppm, Na = 3–4 ppm, K = 1–4 ppm, Ca = 1–2 ppm and Mg = 1 ppm) was composed of polyhedral particles with slightly round edges, and its surface area, S_p, was 15.4 M^2/g. There were small agglomerates consisting of several particles in it, but large ones were not observed. This powder was thoroughly wet-mixed with reagent grade $Mg(NO_3)_2{\cdot}7H_2O$ ($Mg/Al = 1000 \times 10^{-6}$) in ethyl alcohol, dried at 70 °C, calcined at 900 °C for 2 h in flowing O_2 gas, and lightly crushed with an alumina mortar. Batches of the powder were

* Corresponding author at: Strategy Office, National Institute for Materials Science, 1-2-1 Sengen, Tsukuba-shi, Ibaraki 305-0047, Japan.
Tel.: +81 29 859 2000x6827; fax: +81 29 859 2025.
E-mail address: IKEGAMI.Takayasu@nims.go.jp (T. Ikegami).

0272-8842/$36.00
doi:10.1016/j.ceramint.2009.10.002

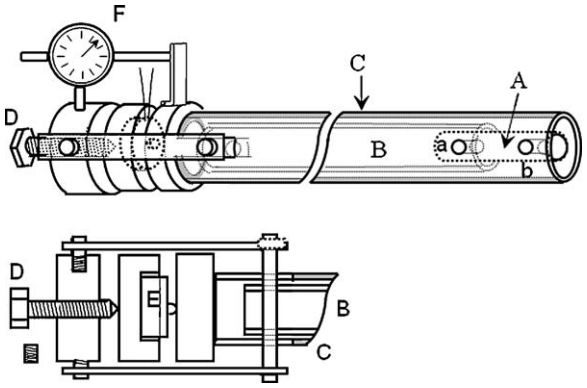

Fig. 1. A schematic of the self-loading apparatus: (A) specimen; (B) inner high alumina tube; (C) outer high alumina tube; (D) bolt; (E) load cell; (F) dial gage; a and b SiC rods.

poured into rubber bags, and then hydrostatically pressed at 200 MPa. The resultant powder compacts were cylinders with a diameter of 20 mm and a length of 150 mm. After being calcined at 900 °C for 2 h, the powder compacts were shaped into simple rods with a suitable radius on a lathe. A hole of 6 mm diameter was made at 10 mm from each end of the specimens on a drill press. The distance between the holes was about 30 mm. Some of the specimens were pre-fired to 1240 °C, 1320 °C and 1360 °C at a heating rate of 1.25 °C/min, and then cooled to room temperature.

Fig. 1 shows a schematic of the loading apparatus. Silicon carbide rods, a and b, with a diameter of 5 mm were used to connect the specimen with the inner and the outer alumina tubes B and C. The bolt D was equipped to adjust the clearances among the specimen and various parts of the apparatus. When the specimen shrank, the compression load cell E was pushed. The dial gauge F monitored shrinkage of the specimen during firing. The part of this apparatus where the specimen was set was placed in the SiC heat element of an electric furnace, and heated at a rate of 10 °C/min to 900 °C, from which the heating rate was changed to 1.25 °C/min. If the specimen was an unfired one, this operation was continued. Just after the load cell indicated a decrease of the load, the loading apparatus was pulled by 150 mm from the furnace to quench the specimen. A pre-fired specimen was, also, set in the loading apparatus and heated by the same method as an unfired specimen. When the temperature rose to a scheduled point, the pre-firing temperature minus 40 °C, a pressure of about 0.5–1.0 MPa was applied to the specimen. Further operations were done again by the same method as that for the unfired specimen.

The apparent sintering stress, σ_{sa}, was computed from

$$\sigma_{sa} = \frac{F_L}{\pi r^2 \rho} \quad (1)$$

where F_L is the measured sintering force, r is the cross-sectional radius of the specimen, and ρ is its relative density. After measurement of F_L, the specimens were cut into several parts such as the part where the tension caused by the sintering force was applied and parts free from the tension concerned. The densities of those parts were measured by the Archimedes method.

The pellets of the powder were formed at 10 MPa with a tungsten carbide die, and hydrostatically pressed at the same pressure as the cylinders for F_L measurement was pressed. The initial relative density, ρ_o, was calculated from the dimensions and weight of the green compact and the theoretical density. Constant-rate-of-heating (CRH) sintering was performed using a thermomechanical analyzer (Model TMA 1700, Rigaku, Tokyo). The ρ of a sintered compact was calculated from Eq. (2) with ρ_o and measured linear shrinkage, $\Delta L/L_o$:

$$\rho = \frac{\rho_o}{(1 - \Delta L/L_o)^3} \quad (2)$$

where L_o is the initial sample length, and ΔL is the difference between L_o and the instantaneous sample length.

3. Results and discussion

The average particle radius of the present powder (49 nm) was evaluated from the equation $R = 3/d_o S_p$ by using the $S_p = 15.4\ M^2/g$, where d_o is the theoretical density of alumina (3.97). Doping MgO decreased ρ_o from 56.5% of the undoped Al_2O_3 powder compact [22] to 54.5%. This decrease in ρ_o suggested that the compressibility of the MgO-doped powder slightly worse while the powder was wet-mixed with the magnesium nitrate in ethanol, dried at 70 °C and calcined at 900 °C. However, the difference in ρ_o between the undoped and the MgO-doped powder compacts was only 2%, and similar packing arrangements of particles were expected for these compacts. The bold curves in Fig. 2 show both densifications of the MgO-doped and the undoped [22] Al_2O_3 powder compacts. The finer curves display the differentials of the densification curves with respect to temperature, $d\rho/dT$. Doping of MgO resulted in a slight shift of the differential curve to higher temperature region.

Fig. 3 shows relative density values before and after sintering force measurement as a function of pre-firing temperature: (○) before the measurement, (□) the part (between the holes a and b in Fig. 1) where the tension caused by the sintering force was applied, ρ_s, and (△) a part (the outer part from the hole a or b) free from the tension, ρ_f. The difference between ρ_f and ρ_s in this figure was about 2% for the

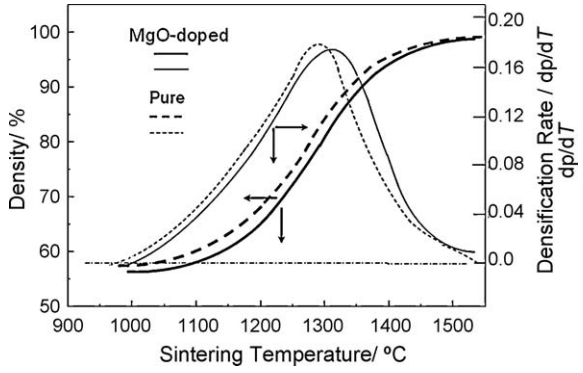

Fig. 2. The densification curves (bold) and the differentials of them (finer) with respect to temperature, $d\rho/dT$ of the Al_2O_3 powders. Solid curves: MgO-doped and broken curves: undoped [22].

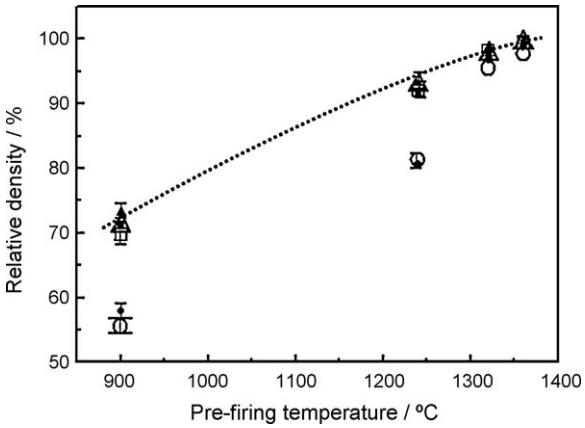

Fig. 3. The relative densities of the MgO-doped (open) and the undoped Al_2O_3 (solid) [22]: (○) and (●) initial; (□) and (■) the part where the tension caused by the sintering force was applied; (△) and (▲) a part free from the tension.

unfired specimen, and decreased to 0.2% for the specimen pre-fired at 1360 °C with increasing pre-firing temperature. The small solid symbols show the previously reported relative densities of the undoped Al_2O_3 specimens [22].

The two-dimensional shrinkage perpendicular to the axial direction was considered for the part of which the axial shrinkage was inhibited by the tension caused by the sintering force. The ρ_s and ρ_f values for the undoped Al_2O_3 specimen were calculated in a previous paper by using a kinetic equation of constant-rate-of-heating sintering [22] under the assumption that the sum of cross-sectional areas of diffusion paths per unit cube is estimated to be proportional to the number of dimensions. The calculated ρ_s and ρ_f values closely fit the small solid symbols in Fig. 3, which indicates similar sintering stresses, σ_s, between the part where the axial shrinkage was inhibited and the parts free from such inhibition.

The dotted curve in Fig. 4 displays the theoretically calculated σ_s [22] from Eqs. (3) and (4), which were respectively derived based on a simple cubic arrangement of grains for the intermediate sintering stage [23] and the packing of tetrakaidecahedra for the final sintering stage [24]. In this calculation, a reported γ for Al_2O_3 (=0.9 N/m) [25] and the reported relationship between ρ and grains size for the undoped Al_2O_3 [26] were used.

$$\sigma_s = \beta_r \gamma (r - r_p) \frac{\left[1 - 2.1(r_p - 0.14r) r_p / (2r - 0.2r_p)\right]}{2r^2} \quad (3)$$

$$\sigma_s = 24 \times \pi r_p \gamma \frac{\{\sin \beta_r / \sin \beta_i\}}{k_s r^2} \quad (4)$$

where r is the average radius of grains, r_p is the pore radius, and β_r and β_i are half the real and the ideal central angles subtending the neck surface, respectively.

The open and the small solid symbols in Fig. 4 show the σ_{sa} of the MgO-doped Al_2O_3 and the undoped Al_2O_3 [22], respectively. The features of σ_{sa} curves of the undoped Al_2O_3 markedly differed from those of the dotted curve. For example, the σ_{sa} values of a pre-fired specimen started from a very small value in spite of a relatively large ρ, quickly increased to its maximum, and then slowly decreased. In contrast, σ_s on the dotted curve in lower ρ region is relatively larger than the σ_{sa}, and abrupt decreases from $\rho = 85\%$. The previous paper [22] indicated that the load cell measured the force causing elastic deformation of various parts of the apparatus especially contacts between parts, the proper sintering stress, σ_s, and the residual stress originating from a preceding sintering force. The proper σ_s can be approximated by the σ_{sa} at the point of contact (hatched circle) between the dotted curve and a σ_{sa} curve or at the inflection point of σ_{sa} curve (hatched triangle). The open circle and the open triangles in this figure were respectively obtained by the same method as the hatched circles and the hatched triangles [22]. The chain curve in Fig. 4 is the curve describing the open circle and the open triangles, approximating the relationship between σ_s and ρ for the MgO-doped Al_2O_3. This figure indicates a considerable reduction of the sintering stress of Al_2O_3 by MgO.

The surface tension, γ, of the MgO-doped Al_2O_3 was calculated from Eqs. (3) and (4) using the previously reported relationship between ρ and grain size [26]. Fig. 5 shows the calculated values of γ together with the reported ones of the

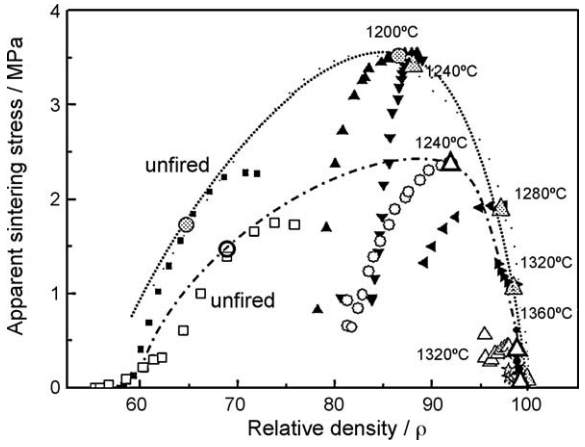

Fig. 4. The apparent sintering stresses, σ_{sa}, of the MgO-doped (open symbols) and the undoped Al_2O_3 (solid symbols) [22]. (○) and (△) σ_s of the MgO-doped, (◍) and (◬) σ_s of the undoped.

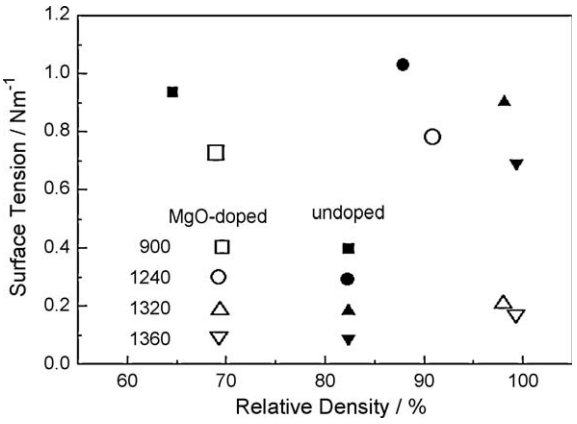

Fig. 5. The surface tensions of the MgO-doped and the undoped Al_2O_3 [22] calculated from Eqs. (3) and (4) with σ_s in Fig. 4.

undoped Al_2O_3. The ratio in γ between the MgO-doped and the undoped Al_2O_3 decreased from 0.75 for the unfired specimens to 0.2 for the specimens pre-fired at 1360 °C.

Reddy and Cooper [16] obtained very close oxygen self diffusion coefficients for undoped and MgO-doped alumina single crystals in a temperature range between 1550 and 1650 °C. The activation energy for the oxygen diffusion was 615 kJ/mol. This value nearly equaled the activation energy, 610 kJ/mol [26], for densification of the undoped and the MgO-doped Al_2O_3 powders between $\rho = 70$–90%. These data suggest a possibility that MgO had a slight influence on the oxygen diffusion coefficient in Al_2O_3. In contrast, Fig. 5 shows a considerable decrease of the surface tension of Al_2O_3 by MgO.

Kinetic equations of sintering [17,18] indicate that the densification rate of a powder compact is proportional to the diffusion coefficient of atoms, the surface tension and the inverse of grain radius. Even if MgO has a slight influence on the oxygen diffusion coefficient in Al_2O_3, it is probable that MgO decreased the densification rate of the Al_2O_3 powder compact by decreasing its surface tension.

The surface tension [27] of a solid varies with the surface orientation. Segregation of an impurity results in decrease of the surface tension of the solid in general. It may be a plausible assumption that the segregation of MgO caused not only large reduction of the surface tensions for larger ones but also small reduction of them for smaller ones. This suggests that MgO decreased the variations between the surface tensions and the grain boundary tensions of Al_2O_3, being well accordance with the reported data [28,29] that MgO narrowed the dispersion of surface-grain-boundary-dihedral angles of Al_2O_3. A previous paper [11] pointed that the narrowing of the concerned dispersion was effective in complete elimination of pores from a sintered body in the final sintering stage.

4. Summary

The sintering forces and the densification of MgO-doped Al_2O_3 were measured using a self-loading apparatus and a thermal mechanical analyzer, respectively. MgO decreased the shrinkage rate and the surface tension of Al_2O_3.

References

[1] R.L. Coble, US Patent 3,026,210 (March 1962).
[2] R.W. Rice, Fabrication of dense MgO, Tech. Rept. NRL-7334, November 1971.
[3] A. Ikesue, T. Kinoshita, K. Kamata, K. Yoshida, Fabrication and optical properties of high-performance polycrystalline Nd:YAG ceramics for solid-state lasers, J. Am. Ceram. Soc. 78 (1995) 1033.
[4] T. Ikegami, J.-G. Li, T. Mori, Y. Moriyoshi, Fabrication of transparent yttria ceramics by the low-temperature synthesis of yttrium hydroxide, J. Am. Ceram. Soc. 85 (2002) 1725.
[5] G. Rossi, J.E. Burke, Influence of additives on the microstructure of sintered Al_2O_3, J. Am. Ceram. Soc. 56 (1973) 654.
[6] G.K. Layden, M.C. McQuarrie, Effect of minor additions on sintering of MgO, J. Am. Ceram. Soc. 42 (1959) 89.
[7] C.H. Hsueh, A.G. Evans, R.L. Coble, Microstructure development during final/intermediate stage sintering. I. Pore/grain boundary separation, Acta Metall. 30 (1982) 1269.
[8] P.J. Jorgensen, J.H. Westbrook, Role of solute segregation at grain boundaries during final-stage sintering of alumina, J. Am. Ceram. Soc. 47 (1964) 332.
[9] J.E. Burke, K.W. Lay, S. Prochazka, The effect of MgO on the mobility of grain boundaries and pores in alumina oxide, Mater. Sci. Res. 13 (1980) 417.
[10] A.H. Heuer, The role of MgO in the sintering of alumina, J. Am. Ceram. Soc. 62 (1979) 317.
[11] T. Ikegami, K. Eguchi, Two kinds of roles of MgO in the densification and grain growth of alumina under various atmospheres: sensitive and insensitive roles to the experimental procedures, J. Mater. Res. 14 (1999) 509.
[12] K.A. Berry, M.P. Harmer, Effect of MgO solute on microstructure development in Al_2O_3, J. Am. Ceram. Soc. 69 (1986) 143.
[13] Y. Oishi, W.D. Kingery, Self-diffusion of oxygen in single-crystal and polycrystalline aluminum oxide, J. Chem. Phys. 33 (1960) 480.
[14] A.E. Paladino, W.D. Kingery, Aluminum-ion diffusion in aluminum oxide, J. Chem. Phys. 37 (1962) 957.
[15] R.H. Doremus, Diffusion in alumina, J. Appl. Phys. 100 (2006) 1.
[16] K.P.R. Reddy, A.R. Cooper, Oxygen diffusion in sapphire, J. Am. Ceram. Soc. 65 (1982) 634.
[17] G.C. Kuczynski, Self-diffusion in sintering of metallic particles, Trans. AIME 185 (1949) 169.
[18] D.L. Johnson, New method of obtaining volume, grain-boundary, and surface diffusion coefficients from sintering data, J. Appl. Phys. 40 (1969) 192.
[19] T. Cheng, R. Raj, Measurement of the sintering pressure in ceramic films, J. Am. Ceram. Soc. 71 (1988) 276.
[20] M.N. Rahaman, L.C.De. Jonghe, R.J. Brook, Effect of shear stress on sintering, J. Am. Ceram. Soc. 69 (1986) 53.
[21] R. Zuo, E. Aulbach, J. Rodel, Experimental determination of sintering stresses and sintering viscosities, Acta Mater. 51 (2003) 4563.
[22] T. Ikegami, N. Iyi, I. Sakaguchi, Evaluation of the sintering force of an Al_2O_3 powder with a self-loading apparatus, Ceram. Int. 35 (2009) 3185.
[23] T. Ikegami, Y. Moriyoshi, Intermediate-stage sintering of a homogeneously packed compact, J. Am. Ceram. Soc. 67 (1984) 174.
[24] R.L. Coble, Sintering crystalline solids. I. Intermediate and final state diffusion models, J. Appl. Phys. 32 (1961) 787.
[25] W.D. Kingery, G. Economos, M. Humenik Jr., Study of metal–ceramic interactions at elevated temperatures, U.S. Atom. Energy Commun. (1953) 83, NYO-3144.
[26] T. Ikegami, M. Yokoyama, Y. Moriyoshi, Effects of MgO on the densification of highly sinterable alumina powders, in: The 43rd Symposium on Basic Science of Ceramics, Chiba, Japan, (2004), p. 338.
[27] J.M. Blakely, Introduction to the Properties of Crystal Surfaces, Pergamon Press, USA, 1973.
[28] T. Ikegami, K. Kotani, K. Eguchi, Some roles of MgO and TiO_2 in densification of a sinterable alumina, J. Am. Ceram. Soc. 70 (1987) 885.
[29] C.A. Handwerker, J.M. Dynys, R.M. Cannon, R.L. Coble, Dihedral angles in magnesia and alumina: distributions from surface thermal grooves, J. Am. Ceram. Soc. 73 (1990) 1371.